Cerebral Cortex, July 2020;30: 3859–3871

doi: 10.1093/cercor/bhaa002
Advance Access Publication Date: 28 January 2020
Original Article

ORIGINAL ARTICLE

Disrupting nNOS–PSD95 Interaction Improves Neurological and Cognitive Recoveries after Traumatic Brain Injury

Wenrui Qu[1,2], Nai-Kui Liu[1], Xiangbing Wu[1], Ying Wang[1], Yongzhi Xia[1], Yan Sun[1], Yvonne Lai[3], Rui Li[2], Anantha Shekhar[4] and Xiao-Ming Xu[1,*]

[1]Department of Neurological Surgery, Spinal Cord and Brain Injury Research Group, Stark Neurosciences Research Institute, Indiana University School of Medicine, Indianapolis, IN 46202, USA, [2]Department of Hand Surgery, The Second Hospital of Jilin University, Changchun, Jilin Province 130041, China, [3]Department of Psychological and Brain Sciences, Indiana University, Bloomington, IN 47405, USA and [4]Department of Psychiatry, Indiana University School of Medicine, Indianapolis, IN 46202, USA

Address correspondence to Xiao-Ming Xu, Spinal Cord and Brain Injury Research Group, Stark Neurosciences Research Institute, Indiana University School of Medicine, 320 West 15th Street, NB Room 500E, Indianapolis, IN 46202, USA. Email: xu26@iupui.edu.

Wenrui Qu and Nai-Kui Liu contributed equally to this work.

Abstract

Excessive activation of N-methyl-D-aspartate receptors (NMDARs) and the resulting neuronal nitric oxide synthase (nNOS) activation plays a crucial role in the pathogenesis of traumatic brain injury (TBI). However, directly inhibiting NMDARs or nNOS produces adverse side effects because they play key physiological roles in the normal brain. Since interaction of nNOS–PSD95 is a key step in NMDAR-mediated excitotoxicity, we investigated whether disrupting nNOS–PSD95 interaction with ZL006, an inhibitor of nNOS–PSD95 interaction, attenuates NMDAR-mediated excitotoxicity. In cortical neuronal cultures, ZL006 treatment significantly reduced glutamate-induced neuronal death. In a mouse model of controlled cortical impact (CCI), administration of ZL006 (10 mg/kg, i.p.) at 30 min postinjury significantly inhibited nNOS–PSD95 interaction, reduced TUNEL- and phospho-p38-positive neurons in the motor cortex. ZL006 treatment also significantly reduced CCI-induced cortical expression of apoptotic markers active caspase-3, PARP-1, ratio of Bcl-2/Bax, and phosphorylated p38 MAPK (p-p38). Functionally, ZL006 treatment significantly improved neuroscores and sensorimotor performance, reduced somatosensory and motor deficits, reversed CCI-induced memory deficits, and attenuated cognitive impairment. Histologically, ZL006 treatment significantly reduced the brain lesion volume. These findings collectively suggest that blocking nNOS–PSD95 interaction represents an attractive strategy for ameliorating consequences of TBI and that its action is mediated via inhibiting neuronal apoptosis and p38 MAPK signaling.

Key words: apoptosis, neuroprotection, N-methyl-D-aspartate receptors, nNOS, PSD95, traumatic brain injury

Introduction

Traumatic brain injury (TBI) afflicts more than 1.5 million individuals each year in the United States of America alone (Loane and Faden 2010; Taylor et al. 2017). Susceptible demographics for TBI include the increasing elderly population, individuals in contact sports, and those involved in military combat. Blast-induced brain injury is a common form of TBI present in the latter category, with a recent study showing the most common cause

of brain injuries in deployed infantry and soldiers in combat are associated with blasts injuries (Regasa et al. 2018). Despite these statistics, treatment options for TBI are limited leaving patients with prolonged cognitive and functional neurologic deficits.

All forms of TBI involve an initial mechanical injury to the brain followed by secondary biochemical events that spread into adjacent tissue and exacerbate damage after the initial primary injury (McIntosh et al. 1996). One of the main contributors to secondary damage following TBI is glutamate excitotoxicity. Glutamate, a common excitatory neurotransmitter, is released into the tissue postinjury and astrocytes within the region respond in effort to reduce this excess glutamate. However, the abundance of glutamate is often too high for effective clearance and induces neuron death through elevated excitatory stimulation. Glutamate stimulates neuronal activation through binding to dedicated glutamate receptors on the neuron surface, as well as via secondary excitatory receptors for N-methyl-D-aspartate (NMDA), AMPA, and kainic acid. Targeting these receptors with antagonist molecules and other means to block glutamate toxicity is a highly studied area in neurological trauma and basic neuroscience.

Among the molecules involved in pathophysiology of TBI, N-methyl-D-aspartate receptors (NMDARs) are considered to be key components. NMDARs are associated with neuronal damage and death (Han et al. 2009; Lai et al. 2014), and NMDAR activation stimulates neuronal nitric oxide synthase (nNOS), which is coupled to the scaffolding protein postsynaptic density protein 95 (PSD95). This reaction instigates production of the signaling molecule nitric oxide (NO), which is implicated in neuronal death and TBI (Castillo et al. 2000; Gahm et al. 2005; Sharma et al. 2006). Despite the role of NMDARs in eliciting this excitotoxicity cascade, direct antagonists of NMDAR are limited in therapeutic potential due to adverse side effects resulting from inhibition of all NMDAR-dependent signaling (Parsons 2001; Chizh and Headley 2005; Lai et al. 2014). Although activation of NMDARs triggers nNOS and PSD95 interaction, disrupting this interaction has different effects on neural survival or death than from directly blocking NMDAR, since the former does not affect NMDARs and the resulting severe side effects. Therefore, developing more specific inhibitors of NMDAR signaling and associated NO signaling is a desirable and promising direction for therapeutic application.

ZL006 is a small molecule endowed with high specificity and potency for disrupting the PSD95–nNOS interaction, and readily crosses the blood–brain barrier (Zhou et al. 2010; Lee et al. 2015; Maccallini and Amoroso 2016; Li et al. 2018). Studies on modulating nNOS–PSD95 in mediating neurological recovery are just emerging. Previously, ZL006 was shown to selectively disrupt the ischemia-induced nNOS–PSD95 interaction and reduce the damage in a mouse stroke model (Zhou et al. 2010). However, the downstream signaling events and functional outcomes were not assessed. In addition, interrupting nNOS–PSD95 interaction promoted neuronal regenerative repair following stroke in rats (Luo et al. 2014) and facilitated recovery from traumatic memory (Li et al. 2018). The role of nNOS–PSD95 interaction in the pathogenesis of TBI the underlying mechanisms and functional efficacies of its intervention, however, remain unclear. In the present study, we investigated the potential neuroprotective role of a small molecule nNOS–PSD95 complex inhibitor ZL006, and determined its mechanism of action in a mouse model of TBI.

Materials and Methods

All of the chemicals used in this study were from Sigma Chemical (St. Louis, MO) except for those specifically indicated. Antibodies used in this study were from Cell Signaling (Boston, MA) except for those specifically indicated.

Animals

Female C57BL/6 mice (10 weeks) were purchased from Jackson Laboratories (Bar Harbor, ME). The animals were maintained on a 12 h/12 h light/dark cycle with food and water freely available. All surgical interventions, treatments, and postoperative animal care were performed in accordance with the Guide for the Care and Use of Laboratory Animals (National Research Council) and the Guidelines of by the Institutional Animal Care and Use Committee of the Indiana University School of Medicine.

Cortical Neuronal Culture, Cell Treatment, and Viability Assessment

Embryonic cortical neurons from embryonic day 18 (E18) Sprague–Dawley (SD) rat or C57BL/6 mouse cortex were dissociated by incubation in 0.05% trypsin/EDTA followed by gentle trituration as described previously (Han et al. 2004). The cells were grown in serum-free Neurobasal medium supplemented with 2% B27 and 0.05 mmol/L glutamine (Life Technologies, Inc.). Three days later, 5 μM cytosine-D-arabinofuranoside was added to the medium for 24 h to inhibit glial cell division. Under this culture condition, a purity of greater than 85% cortical neuronal population was obtained at the seventh day in vitro. At 7 days in culture, rat cortical neurons were exposed to 100 μM glutamate for 24 h to induce cell death. To assess the protective effects of ZL006, cells were pretreated with 0.1, 1, and 10 μM ZL006 for 30 min followed by replacement with medium with and without glutamate. Cell death was evaluated in cultured cortical neurons using a propidium iodide (PI) inclusion assay and lactase dehydrogenase (LDH) release following ZL006 and glutamate treatments. After 24 h of treatment, the culture medium of each well was removed for LDH release using a nonradioactive LDH cytotoxicity assay kit (Promega). For the PI inclusion assay, Hoechst 33342 (5 μg/mL) was added to the cells at 37 °C for 15 min to label all cell nuclei, followed by incubation with 5 μg/mL PI for 10 min to stain the nuclei of dead cells. The cells were washed with phosphate-buffered saline (PBS) and then fixed with 4% paraformaldehyde (PFA) for 10 min. The fixed cells were washed with PBS and were imaged with an inverted OlympusIX71 fluorescence microscope (Olympus America Inc.). The percentage of PI positive/Hoechst positive cells was counted using an ImageJ software. To be clinically relevant, ZL006 (1.0 and 10 μM) was added to mouse cortical neuronal culture at 30 min after the glutamate administration. At 24 h after the glutamate treatment, the mouse cortical neurons from each well were collected for coimmunoprecipitation (Co-IP) analysis and cell culture medium from each well was removed for the LDH release assay.

Traumatic Brain Injury and Treatment

The mouse controlled cortical impact (CCI) model was selected because the light body weight of mice is attractive for testing therapeutic interventions. In addition, transgenic and

knockout mice are available for the study of genetic and molecular mechanisms. Mice were randomly divided into sham, TBI and treatment groups. The CCI model in mice was performed according to our previous report (Liu et al. 2014b). Briefly, mice were anesthetized with Avertin (2.5%, 0.2 mL/20 g) and were placed in a stereotactic frame adapted for mice. A midline incision was made to expose the skull, and a 4.5 mm diameter craniotomy was performed midway between the bregma and lambda, and 2.5 mm lateral to the midline over the left hemisphere. Mice were subjected to a standardized CCI injury protocol—1.0 mm impact depth using an electromagnetic impactor (Impactor OneTM, MyNeuroLab; round tip: 3 mm diameter; speed: 3 m/s; dwell: 50 ms). After injury, the skin incision was closed with 5–6 interrupted sterile 4–0 nylon sutures. Triple antibiotic ointment was applied to the skin. For the sham-operated controls, the animals received the same anesthesia and surgical procedure (craniotomy) without the impact. The animals were kept on a heating pad throughout the surgery. After surgery, the animals were put into cages on the heating pad until they recovered from anesthesia. At 30 min after contusion injury, mice were treated with ZL006 (10 mg/kg, i.p.) or vehicle. At 24 h after CCI, they were sacrificed for Western blot analysis, coimmunoprecipitation, immunofluorescence labeling, and TUNEL staining. For long-term neuroprotective effects, ZL006 (5 and 10 mg/kg) and vehicle were delivered intraperitoneally at 30 min postinjury and daily thereafter up to 7 days. Following the injury, mice were subjected to a variety of cognitive and behavioral tests, and were sacrificed for histopathological examination 4 weeks later.

Western Blot Analysis

Western blot analysis was performed on homogenized cortex as modified from previously described (Liu et al. 2004, 2014a). Briefly, proteins were extracted from the mouse cortex at 24 h postinjury in radioimmunoprecipitation assay buffer supplemented with Halt protease and phosphatase inhibitor cocktail (Thermo Scientific, Rockford, IL). Forty microgram proteins were electrophoresed on a 7–12% sodium dodecyl sulfate-polyacrylamide gel, transferred onto a nitrocellulose membrane, and immunoblotted with the following primary antibodies:rabbit anticleaved PARP-1 (1:500), rabbit anticleaved-caspase-3 (1:1000), rabbit anti-Bcl-2 (1:100, Santa Cruz Biotechnology, Dallas, TX), rabbit anti-Bax (1:100, Santa Cruz Biotechnology), mouse anti-Drp1 (1:1000), rabbit anti-phospho-Drp1 (Ser616) (1:100), rabbit anti-ERK1/2 (1:1000), mouse anti-p-ERK1/2 (1:2000), rabbit anti-p38 (1:100), mouse anti-phospho-p38 (1:1000), and mouse anti-β-tubulin (1:1000, Sigma). The next day, the membranes were washed and incubated with secondary Alexa Fluor 680 goat anti-mouse (1:5000, Invitrogen, Grand Island, NY) and IRDye 800 goat anti-rabbit (1:5000, Rockland, Gilbertsville, PA) antibodies. The Western blots were imaged and quantified using a Li-Cor Odyssey Infrared Imaging system (LI-COR Biosciences) according to the manufacturer's instruction.

Coimmunoprecipitation

Lysis and coimmunoprecipitation (Co-IP) of cultured cortical neurons or mouse cortices were performed with Pierce Classic IP Kit (Thermo Scientific, Rockford, IL) according to the manufacturer's instruction. Briefly, the mouse cortices were homogenized in ice-cold lysis buffer (25 mM Tris, 150 mM NaCl, 1 mM EDTA, 1% NP-40, 5% glycerol, pH 7.4) supplemented with Halt protease and phosphatase inhibitor cocktail (Thermo Scientific, Rockford, IL). For neuronal culture, the ice-cold IP Lysis/Wash Buffer (300 µL) supplemented with Halt protease and phosphatase inhibitor cocktail (Thermo Scientific) was added to the cells for incubation on ice for 5 min with periodic mixing. The lysate was centrifuged at 13 000$\times g$ for 10 min at 4 °C. The supernatants were preincubated with 25 µL of control agarose resin for 1 h at 4 °C and then centrifuged to remove proteins that adhered nonspecifically to the resin. Mouse-anti nNOS antibody (Transduction Laboratories) at 2 µg per 100 µg of total protein was added to the supernatant and incubated overnight at 4 °C. Then, the antibody/lysate sample was added to protein A/G agarose and incubated at 4 °C for 1 h. Immune complexes were isolated by centrifugation, washed five times with lysis buffer, and bound proteins were eluted by heating at 95 °C in loading buffer for 10 min for immunoblotting. Proteins were analyzed by Western blot using rabbit anti-PSD-95 (1:1000) or rabbit anti-nNOS (1:1000).

TUNEL Staining

Apoptotic cortical neurons were detected by TUNEL and the immunostaining of the neuronal marker NeuN using an in situ cell death detection kit (TMR red; Roche Applied Science), according to the manufacturer's instructions. Briefly, 10 sections spanning the lesion area were double labeled with mouse anti-NeuN antibody (1:200, Millipore Inc.) and In Situ Cell Death Detection Kit, TMR red (Roche Diagnostics) according to the manufacturer's instructions. A secondary goat anti-mouse Alex488 antibody was incubated to label NeuN positive cells. TUNEL positive cells were labeled red. Colabeled cells in the penumbral region in each section for each animal were counted and the percentage TUNEL-positive neurons was quantified using an Olympus BX60 fluorescent microscope and ImageJ software.

Immunofluorescence Labeling

Brain tissue was dissected and sectioned as described above at 1 day post-TBI, and double immunofluorescence labeling was performed as described previously (Liu et al. 2014a). A set of cryosections were used for immunofluorescence double labeling of NeuN, a marker for neuron, and phosphorylated-p38 MAPK (p-p38). In brief, sections were hydrated in PBS, permeabilized with 0.3% Triton X-100 in PBS (PBST) and blocked with 0.3% Triton X-100/10% normal goat serum (Vector Labs) for 1 h at room temperature. Next, the sections were incubated with mouse anti-NeuN (1:200, Millipore) and rabbit anti-p-p38 (1:200, Cell Signaling, Inc.) overnight at 4 °C. The next day, the sections were incubated with TRITC-conjugated goat anti-rabbit and Alexa Fluor 488-conjugated goat anti-mouse secondary antibodies (both 1:200, Jackson Immuno Research). Five random fields of view per section were imaged and NeuN/p-p38 double labeled cells were quantified using an Olympus BX60 fluorescent microscope and ImageJ software.

Behavioral Assessments

All behavioral tests were blindly performed. Following surgery, the groups underwent a battery of functional assessments to test sensorimotor and cognitive abilities beginning as early as 2 days postsurgery and weekly thereafter for 4 weeks.

Neuroscore

A composite neuroscore test was conducted to assess the neurological motor function of mice according to an established protocol (Liu et al. 2013, 2014b). Mice were given an integer score from 0 (severely impaired) to 4 (normal) for each of the following indices: forelimb function, hindlimb function, and resistance to lateral pulsion.

Rotarod

Assessment of sensorimotor function and coordination of the mice was performed using a Rotarod test as previously described (Liu et al. 2013, 2014b). Briefly, each mouse was placed on a rotating drum and the time each animal was able to maintain its balance walking on the rod before falling was recorded. The latency to balance on a rotating rod was measured at a rotational acceleration using a five-lane rotarod device (IITC Life Science, Inc.). The device was accelerated from 1 to 18 rpm over 90 s, with each trial lasting a maximum of 120 s. Trials ended when mice either fell off the rod or clung to the rod as it made one complete rotation.

Adhesive Removal Test

The adhesive removal test for sensorimotor function was performed according to our established protocol (Liu et al. 2013, 2014b). In brief, a small piece of adhesive tape (waterproof adhesive tape, ACME/CHASTON, Dayville CT) was placed on the right forepaw of the mice and the time it took the animal to attempt to remove the tape (time-to-contact) and the time until full removal (time-to-removal) were measured.

Morris Water Maze

The memory and cognitive function of the mice were tested using a Morris Water Maze as described previously (Morris et al. 1982; Cai et al. 2011; Liu et al. 2013, 2014b). In brief, the maze was consisted of a plastic pool (100 cm diameter, 60 cm depth) filled with water to a depth of 26.5 cm. A clear Plexiglas stand (10 cm diameter and 26 cm height) was used as the hidden goal platform. Mice were trained before TBI for five consecutive days (four trials per day). A time of 60 s maximum was allowed for each mouse to find the platform. If a mouse did not find the platform in the allotted time, it was gently placed on the platform for 30 s before being placed in a heated incubator between trials (4 min intertrial interval). Testing began on postoperative day 15 to avoid possible confounds with motor deficits observed in the first few days postinjury. The mice were subjected to four trials per day for four consecutive days (days 15–18). For each daily set of four trials, mice were placed in the pool facing the wall. Trials were randomly started from four possible start locations (north, east, south, and west). The time required (latency) to find the platform with a 60 s limit was recorded and tracked using TOPSCAN software (Clever Sys Inc.). If a mouse failed to find the platform within the allotted timeframe, it was treated as described for preinjury training. A single, 60 s probe trial was performed 24 h following the final learning trial. To control for visual discrimination or motor impairment, the same animals were finally required to locate a cued platform with a ball that extended above the water surface by 12 cm.

Social Memory Assessment

"Social memory interaction assessment" followed procedures described previously (Thor and Holloway Jr 1986; Yang et al. 2013; Martos et al. 2017) with minor modification. Mice were placed into fresh homecage and allowed to habituate to the new environment for 15 min. A stimulus mouse (same sex and similar age as the test subject) taken from a different homecage was introduced into the cage with the test subject as a social cue for an initial interaction trial of 5 min. The intervals between the initial trial and social memory test were 30 min, 3 h, or 6 h. After the selected separation period, the test subject was returned to the test cage with either the familiar or a novel stimulus mouse for the 5-min recognition test. The social investigation was observed continuously by a trained observer who timed the duration of investigation behaviors. Investigation behaviors include direct contact with the stimulus mouse while inspecting any part of the body surface (including grooming, licking, and pawing); sniffing of the mouth, ears, tail, or ano-genital area; and closely following (within 1 cm) the stimulus mouse. Any aggressive and sexual behaviors were excluded.

Histological Assessments

Brain histology processing and analysis for ZL006 effects on lesion volume were performed as previously described (Liu et al. 2013, 2014b). Briefly, 4 weeks post-TBI, mice were deeply anesthetized, perfused with PBS followed by 4% PFA, and the brains dissected out, embedded, and sectioned at 25 μm thickness on a cryostat. A set of serial cross sections of the brain were stained with Cresyl Violet, and for each section, the contours of the bilateral hemispheres, cortices, and hippocampi were traced, and the areas were measured using an Olympus BX60 microscope. Volumes were calculated according to the Cavalieri principle (Coggeshall 1992). Tissue loss was obtained by subtracting the volume of remaining ipsilateral tissue from contralateral tissue according to an established protocol (Liu et al. 2014b). Percent of volumetric tissue loss was calculated by the ratio of the tissue loss divided by the contralateral tissue measure. Surviving neurons were counted in the CA1 hippocampal region under a light microscope at $\times 20$ magnification. Cells were calculated from three sections of the CA1 hippocampus within a dissector area of 900 μm^2 (30×30 μm) randomly positioned by the software (Image pro plus 6.0) over the region of interest. Nine squares were counted from three sections per mice brain. The results were expressed as cell density per $100 \mu m^2$.

Statistical Analysis

All data are presented as mean ± SEM. One-way ANOVA with Tukey post hoc analysis was performed to determine statistical significance between multiple groups. The behavior scores at various time-points postinjury were examined using repeated measures ANOVA (time) with the group factor (injury groups), followed by post hoc *t*-tests, where appropriate. A student's unpaired *t*-test was utilized to compare the means of two groups. A P value < 0.05 was considered statistically significant.

Results

ZL006 Protects Primary Cortical Neurons from Glutamate-induced Excitotoxicity

First, we determined whether disruption of nNOS–PSD95 interaction with ZL006 was neuroprotective against glutamate-induced toxicity in primary cortical neurons (Fig. 1). Glutamate induced cell death, as measured by PI staining of nuclei acids in dead cells. Pretreatment of neuronal cells with ZL006 (0.1, 1.0, and 10 μM) significantly reduced neuronal cell death in a

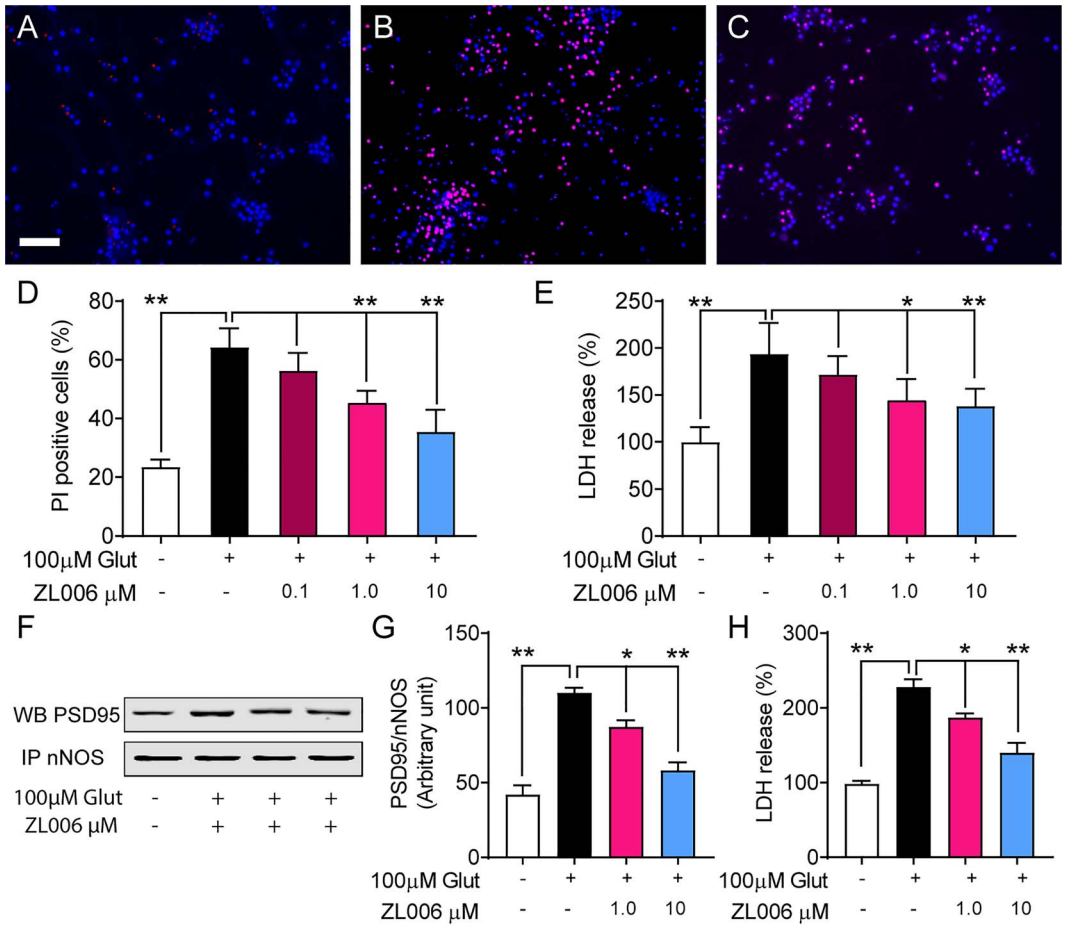

Figure 1. ZL006 protects cortical neurons from glutamate-induced cell death in vitro. After exposure to glutamate (Glu, 100 μM) for 24 h, rat cortical neuronal death, measured by PI staining (*B*, *C*, red) was markedly increased compared with nonglutamate treated cells (*A*). Pretreatment with ZL006 significantly reduced rat neuronal cell death (*C*, *D*), as compared with the Glu-treated cells (*B*, *D*). LDH release assay showed that ZL006 pretreatment significantly reversed Glu-induced rat cortical neuronal death (*E*). $^{*}P < 0.05$; $^{**}P < 0.01$ (One-way ANOVA with multiple comparisons test, $n = 5$–7). Scale bar = 50 μm. Data represent the mean ± SEM from three independent experiments. (*F*–*H*) Mouse cortical neurons were used for post-treatment of ZL006 after glutamate stimulation. (*F*) Representative images of coimmunoprecipitation (Co-IP). Samples were immunoprecipitated (IP) and analyzed using western blotting (WB). ZL006 was added at 30 min after the glutamate stimulation, and the proteins were isolated at 24 h after the glutamate treatment for the Co-IP analysis. (*G*) The bar graph shows that the ZL006 post-treatment significantly reduced glutamate-induced nNOS–PSD95 complex in a dose-dependent manner, as compared with the glutamate-treated cells without ZL006 treatment. $^{*}P < 0.05$; $^{**}P < 0.01$ (One-way ANOVA with multiple comparisons test, $n = 4$). (*H*) LDH release assay showed that ZL006 post-treatment at 30 min postglutamate stimulation significantly reversed glutamate-induced cortical neuronal death. $^{*}P < 0.05$; $^{**}P < 0.01$ (One-way ANOVA with multiple comparisons test, $n = 6$). Data represent the mean ± SEM from three independent experiments.

dose-dependent manner (Fig. 1A–D). When neuronal cell death was measured by LDH, a stable cytoplasmic enzyme that is present in all cells but only released when the plasma membrane is damaged, glutamate increased LDH release at 24 h. Pretreatment of ZL006 also significantly reduced cell death in a dose-dependent manner (Fig. 1E). To clinically relevant, we further examined the effects of ZL006 on nNOS–PSD95 interaction and neuronal death in mouse cortical neurons at 30 min after glutamate stimulation. Our results showed that post-treatment of ZL006 at 30 min after glutamate stimulation significantly reduced glutamate-induced nNOS–PSD95 complex in a dose-dependent manner (Fig. 1F,G). LDH analysis further showed that post-treatment of ZL006 significantly reduced neuronal death in a dose-dependent manner (Fig. 1H). These data collectively indicate that disrupting nNOS–PSD95 interaction with ZL006 is neuroprotective on cortical neurons in response to glutamate-induced excitotoxicity in vitro.

ZL006 Disrupts nNOS–PSD95 Complex, and Attenuates Apoptosis after TBI

To further assess the role of nNOS–PSD95 interaction in TBI, we investigated the effect of ZL006 on nNOS–PSD95 complex and apoptosis in a mouse model of CCI. Co-IP analysis showed a significant increase in the expression of nNOS–PSD95 complex at 1 day after TBI ($P < 0.01$, Fig. 2A) and such increased nNOS–PSD95 complex could be reversed by administration of ZL006 (10 mg/kg, i.p.) at 30 min postinjury ($P < 0.01$, Fig. 2A). Western blot analysis showed that administration of ZL006 (10 mg/kg, i.p.) at 30 min postinjury also significantly reduced TBI-induced biomarkers of apoptosis including active PARP (Fig. 2B), active caspase-3 (Fig. 2C), and ration of Bcl-2/Bax (Fig. 2D) in the cortex after TBI as compared with the vehicle treatment, suggesting that ZL006 attenuates apoptosis by disrupting the nNOS–PSD95 complex. TUNEL staining with a neuron marker NeuN further showed a

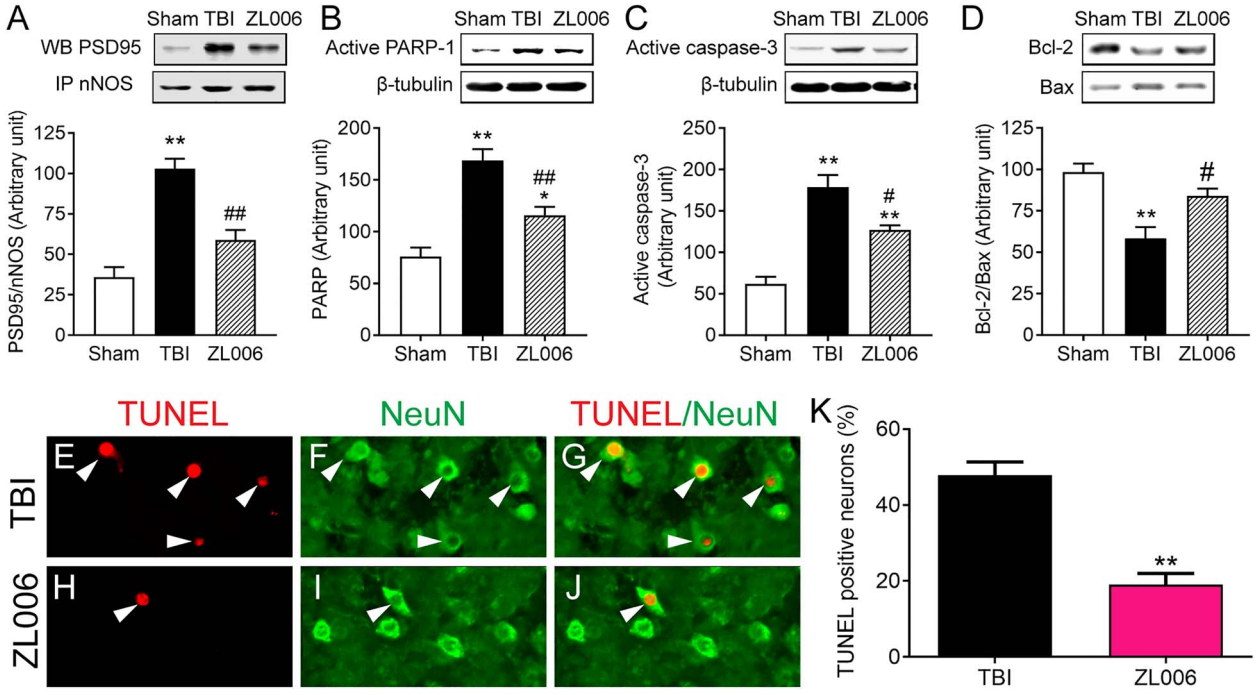

Figure 2. ZL006 reduces the nNOS–PSD95 complex and cortical neuronal apoptosis at 1 day post-TBI. (*A*) Coimmunoprecipitation (Co-IP) analysis shows levels of the nNOS–PSD95 complex in the cortex of mice with TBI and sham. Samples were IP and analyzed by WB. The bar graph shows ZL006 administration (10 mg/kg, i.p.) at 30 min postinjury significantly reduced TBI-induced the nNOS–PSD95 complex in the cortex at 1 day postinjury. $^{**}P < 0.01$ vs sham; $^{\#\#}P < 0.01$ vs TBI. (One-way ANOVA with multiple comparisons test, $n = 3$ mice/group). Data represent the mean ± SEM. (*B–D*) Western blot analysis shows that administration of ZL006 (10 mg/kg, i.p.) at 30 min postinjury significantly reduced TBI-induced active caspase-3 (*B*), active PARP (*C*) and ratio of Bcl-2/Bax (*D*) in the cortex at 1 day postinjury as compared with the TBI vehicle treatment. $^{**}P < 0.01$ vs sham; $^{\#}P < 0.05$, $^{\#\#}P < 0.01$ vs TBI. (One-way ANOVA with multiple comparisons test, *B*, $n = 5$; *C*, *D*, $n = 4$ mice/group). Data represent the mean ± SEM. (*E–K*) TUNEL staining (*E* and *H*, arrow head) was localized in neuron with NeuN-IR (*F* and *I*, arrow head) as seen in the merged image (*G* and *J*, arrow head). The bar graph in *K* shows that the ZL006 administration (10 mg/kg, i.p.) at 30 min postinjury significantly reduced TBI-induced neuronal apoptosis in the cortex at 1 day postinjury. $^{**}P < 0.01$ vs TBI (Student *t*-test, $n = 5$ mice/group). Data represent the mean ± SEM.

significantly reduction in the number of TUNEL-positive neurons in the injured cortex treated with ZL006 (Fig. 2*H–K*) as compared with untreated TBI (Fig. 2*E–G,K*) ($P < 0.01$), providing evidence of the antiapoptotic effect by disrupting the nNOS–PSD95 interaction.

ZL006 Reduces TBI-induced Neuronal Activation of p38 MAPK

Previously, nNOS–PSD95 interaction was shown to mediate glutamate-stimulated p38 MAPK activity and subsequently neuronal death (Cao et al. 2005). We thus determined the effect of ZL006 on phosphor-p38 MAPK (p-p38), a marker of activated p38 MAPK, in cortical neurons at 1 day after TBI. Immunofluorescence double labeling of p-p38 and NeuN showed that TBI induced a significant increase in the number of p-p38 positive cortical neurons adjacent to the injury site ($P < 0.01$) (Fig. 3*D–F,J*) as compared with the sham control (Fig. 3*A–C,J*). ZL006 administration (10 mg/kg, i.p.) at 30 min postinjury significantly reduced the number of p-p38 positive neurons after TBI ($P < 0.05$) (Fig. 3*G–I,J*). Western blot analysis showed that administration of ZL006 (10 mg/kg, i.p.) at 30 min postinjury significantly reduced TBI-induced p-p38 activation (Fig. 3*K*) in the cortex at 1 day after TBI as compared with the TBI vehicle treatment ($P < 0.01$).

ZL006 Improves Sensorimotor Function after TBI

Neuroscore, Rotarod, and Adhesive removal tests were performed on consecutive days following TBI to evaluate motor and sensorimotor function in all groups. Neuroscores were significantly decreased after TBI (Fig. 4*A*, $P < 0.01$). This decrease began at 2 day postinjury and persisted for the entire duration of the study when compared with sham mice (Fig. 4*A*, $P < 0.01$). Such decreases in neuroscore were reversed by ZL006 in a dose-dependent manner (Fig. 4*A*, $P < 0.05$–0.01). Rotarod performance showed significant deficits after TBI as compared with sham mice during the entire investigation period (Fig. 4*B*, $P < 0.01$). ZL006 treatments at both doses (5 and 10 mg/kg) significantly improved rotarod performance (Fig. 4*B*, $P < 0.01$). The adhesive removal test was used to examine paw and mouth sensitivity (contact time) and dexterity (removal time) (Liu et al. 2013, 2014b). The adhesive removal test showed significant deficits after TBI during the entire investigation period (Fig. 4*C*, $P < 0.01$) in terms of contact time, a measure of diminished somatosensory function. ZL006 at 5 mg/kg showed an improvement in the contact time at 2 and 4 weeks postinjury as compared with the TBI alone group (Fig. 4*C*, $P < 0.05$) while ZL006 treatment at 10 mg/kg showed only a trend in improvement in the contact time compared with the vehicle group (Fig. 4*C*). In the removal test, removal time was also increased in the TBI during the entire investigation period, as compared with the sham group (Fig. 4*D*, $P < 0.01$). ZL006

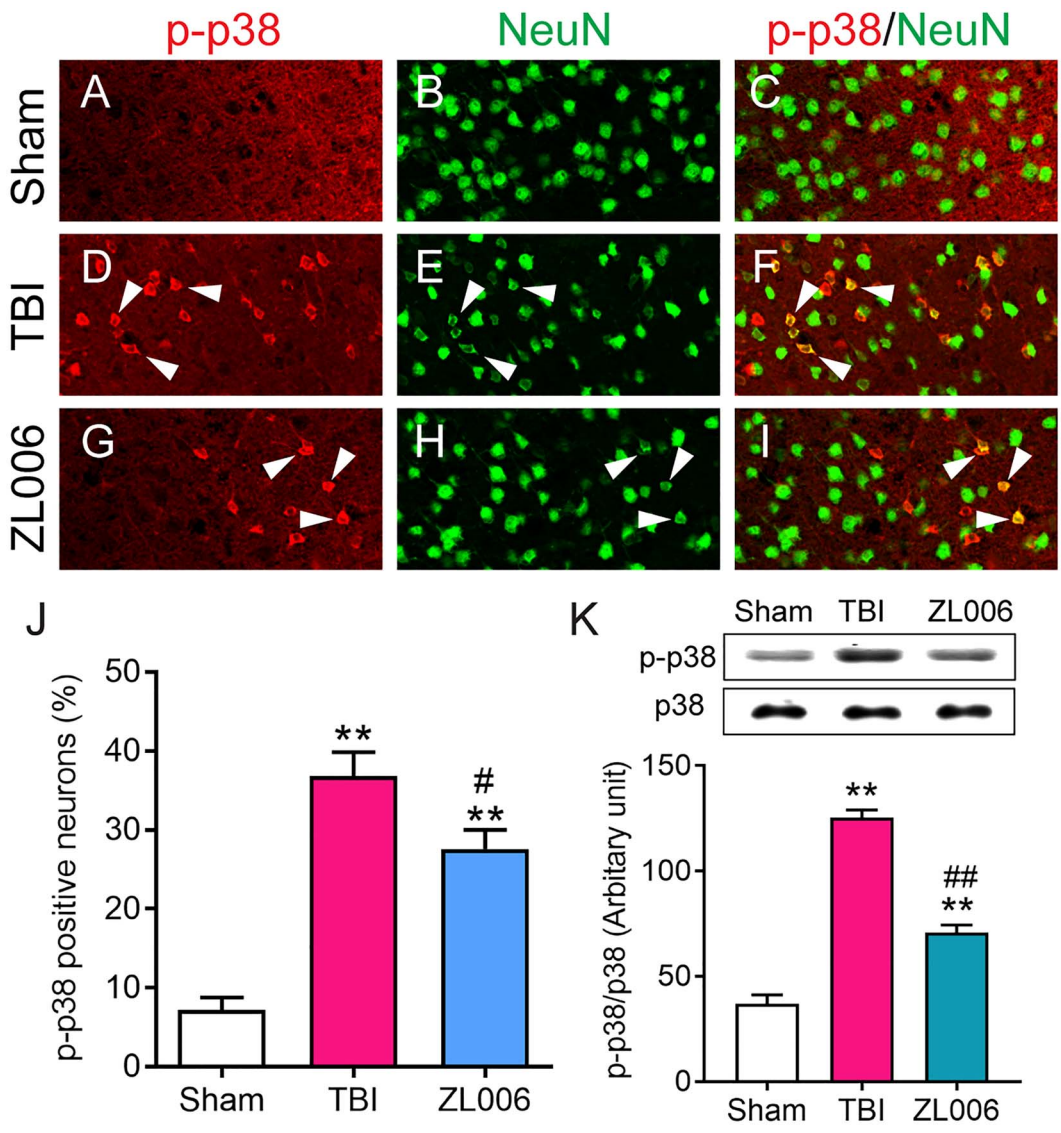

Figure 3. ZL006 reduces p38 MAPK expression at 1 day after TBI. Phospho-p38 MAPK (p-p38)-IR (*A*, *D*, *G*, arrow heads) was localized in neuron with NeuN-IR (*B*, *E*, *H*, arrow heads) as seen in the merged image (*C*, *F*, *I*, arrow heads). *J*, Bar graph shows administration of ZL006 (10 mg/kg, i.p.) at 30 min postinjury significantly reduced TBI-induced p-p38 expression in the cortex. $^{**}P < 0.01$ vs sham; $^{\#}P < 0.05$, vs TBI. (One-way ANOVA with multiple comparisons test, $n = 5$ mice/group). Data represent the mean ± SEM. Western blot analysis shows that administration of ZL006 (10 mg/kg, i.p.) at 30 min postinjury significantly reduced TBI-induced p-p38 expression (*K*) in the cortex as compared with the TBI vehicle treatment. $^{**}P < 0.01$ vs sham; $^{\#}P < 0.05$, $^{\#\#}P < 0.01$ vs TBI. (One-way ANOVA with multiple comparisons test, $n = 6$ mice/group). Data represent the mean ± SEM.

treatment significantly reversed this increase at 2–4 weeks post-TBI (Fig. 4D, $P < 0.05$ and $P < 0.01$), indicating that ZL006 improves sensory and motor function.

ZL006 Treatment Improves Spatial Memory and Learning after TBI

Prior to TBI, no significant difference between the groups was observed in the latency to find the hidden platform in the Morris water maze assessment (Fig. 5A) and no significant difference was found between the groups in swim speed (data not shown). However, a significantly increased latency was detected after TBI when compared with sham (Fig. 5B). ZL006 treatment at both doses significantly reduced the increased latency after TBI (Fig. 5B, $P < 0.05$ and $P < 0.01$). These results could be appreciated in a density map for each group of the time spent in given areas of the maze, with the circle representing the platform and the red indicating the most time spent (Fig. 5C). The probe test further revealed that ZL006 significantly reduced the average distance to the target (Fig. 5D) and the time to the target (Fig. 5E), as well as increased the number of crossings (Fig. 5F) and traveled distances (Fig. 5G) after TBI in a dose-dependent manner ($P < 0.05$ and $P < 0.01$).

ZL006 Improves Social Memory after TBI

As TBI can potentially affect social memory, we assessed this ability in the mice using a specific social memory test to determine if ZL006 had any impact on this aspect of memory. To characterize the effect of ZL006 on social interaction after TBI,

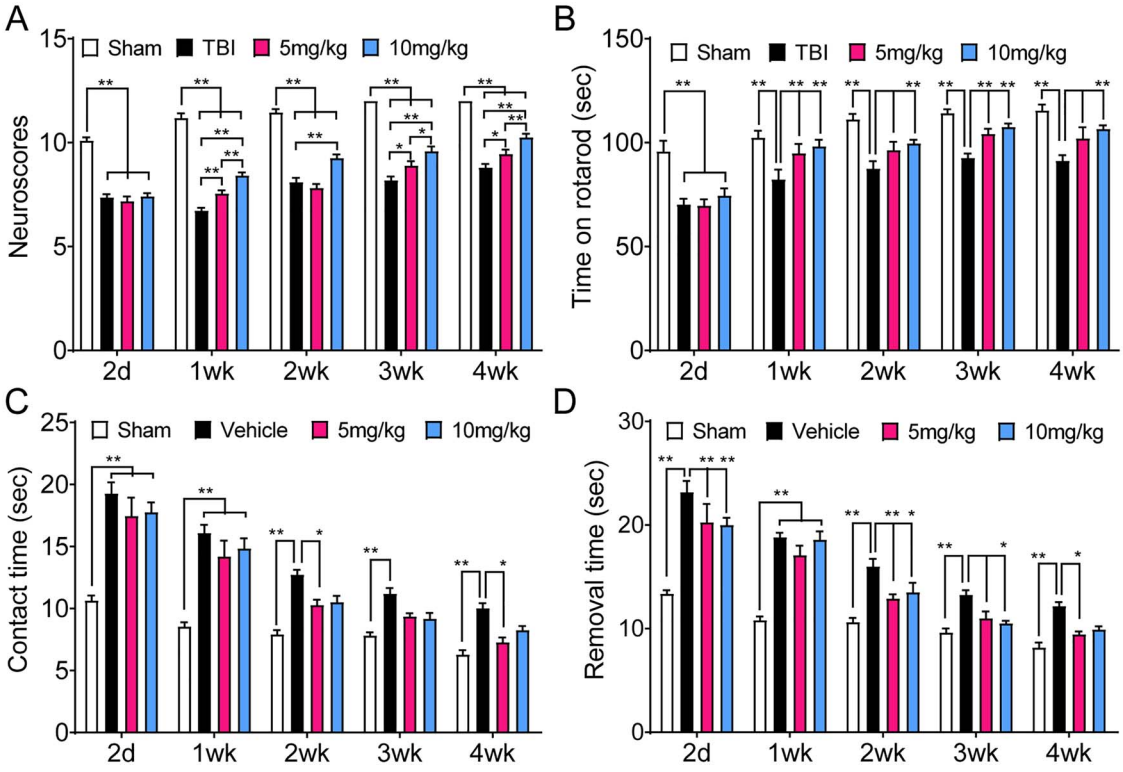

Figure 4. ZL006 improves sensorimotor function after TBI. (*A*) Composite neuroscores, assessed up to 4 weeks after TBI. ZL006 (10 mg/kg, i.p,) significantly increased the neuroscores following TBI as compared with the TBI alone group. (*B*) ZL006 treatment significant improved rotarod performance as compared with the TBI alone. (*C*, *D*) Adhesive removal test performed up to 4 weeks after TBI. Time-to-contact the adhesive tape on the paw (*C*) and time-to-remove the adhesive tape from the paw (*D*) were significantly improved after ZL006 treatment compared with nontreated animals. $^{*}P < 0.05$, $^{**}P < 0.01$ (Two-way repeated measures ANOVA with multiple comparisons test, $n = 11$–12 mice/group). Data represent the mean ± SEM.

mice were placed into fresh homecage and allowed to habituate to the new environment for 15 min. A stimulus mouse (same sex and similar age as the test subject) taken from a different homecage was introduced into the cage with the test subject as a social cue for an initial interaction trial of 5 min. The intervals between the initial trial and social memory test were 30 min, 3 h, or 6 h. After the selected separation period, the test subject was returned to the test cage with either the familiar or a novel stimulus mouse for the 5 min recognition test. In the sham group, mice spent significantly more time with the familiar than the novel stimulus mouse (Fig. 6A, $P < 0.01$). After a 6 h delay after the initial interaction, the test mouse with TBI spent the same amount of time investigating the same social cue mouse as in the initial trial (Fig. 6B), indicating deficits in social memory. In contrast, the ZL006 treatment group at dose of 10 mg/kg spent significantly more time with the familiar than the novel stimulus mouse even after 6 h (Fig. 6D), similar to the sham (Fig. 6A), suggesting that ZL006 improves social memory after TBI.

ZL006 Reduces Lesion Volume Following TBI

To further access whether disrupting nNOS–PSD95 interaction with ZL006 reduce tissue damage after TBI, histologic sections of brain tissue were stained with Cresyl violet and lesion volumes were measured. Following assessment of histological properties of the lesion after TBI, no histological evidence of injury to the brain in sham-operated mice was observed (Fig. 7A). After TBI, there was a loss of cortical tissue (Fig. 7B). A bar graph demonstrated that administration of ZL006 (5 and 10 mg/kg, i.p.) at 30 min postinjury and daily thereafter up to 7 days significantly reduced volumetric tissue lose in the cortex in a dose-dependent manner at 4 weeks after TBI (Fig. 7A–E) ($P < 0.01$). To access whether deficits of spatial memory and learning after TBI is related to hippocampal neuronal death, we also counted neurons in the CA1 region of the hippocampus. After TBI, neuronal loss in the CA1 region was clearly observed (Fig. 7F). Administration of ZL006 significantly reduced neuronal lose in the CA1region in a dose-dependent manner at 4 weeks after TBI (Fig. 7F) ($P < 0.01$).

Discussion

To our knowledge, this is the first study demonstrating that disrupting nNOS–PSD95 interaction with a small molecule ZL006 resulted in neuroprotection and functional recovery after TBI in adult mice, as illustrated in Figure 8. Our in vitro data show that ZL006 disrupted nNOS–PSD95 interaction and reduced glutamate-induced excitotoxicity to cortical neurons and protected them from apoptotic death in a dose-dependent manner. We provide direct evidence that administration of ZL006 disrupted nNOS–PSD95 interaction and reduced neuronal apoptosis in a mouse model of TBI. Notably, we demonstrate that ZL006's effect is mediated through inhibition of p38 MARK activation after TBI, revealing a molecular mechanism underlying the nNOS–PSD95 interaction. Most importantly,

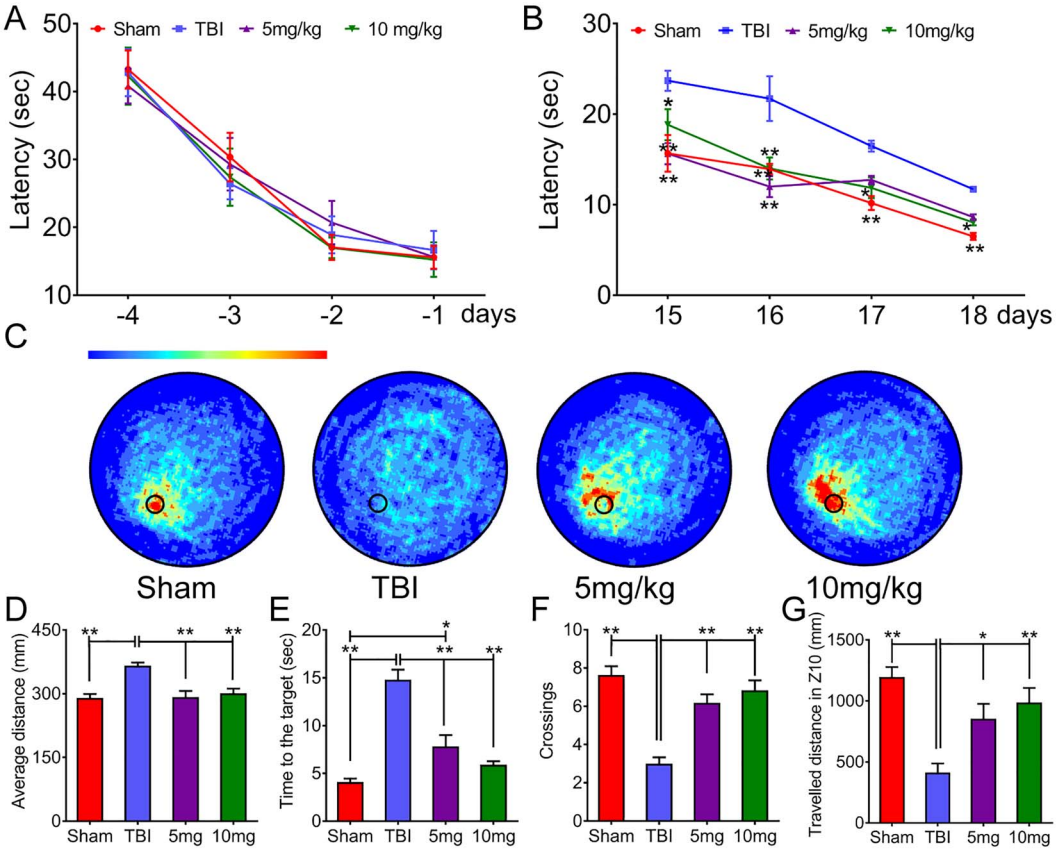

Figure 5. ZL006 improves spatial memory and learning after TBI. (*A*) Before TBI, no significant difference in latency of platform location was observed between groups in the Morris water maze test. (*B*) After TBI, significant memory deficit was found in the TBI group as compared with the sham group. Notably, the ZL006 group showed a significant improvement (reduced latency) as compared with the TBI group. $^{*}P < 0.05$, $^{**}P < 0.01$ vs TBI (Two-way repeated measures ANOVA with multiple comparisons test, $n = 11$–12 mice/group). (*C*) Density heat maps for grouped data showing where sham and experimental mice concentrated their searches in the probe test, with the circle representing the platform and red indicating the most time spent. Color bar: red and yellow regions represent areas of high occupancy; green and blue represent areas of low occupancy. (*D*–*G*) Bar graphs show that ZL006 treatment significantly reduced the average distance to the target (*D*) and the time to the target (*E*), as well as increased the number of crossings (*F*) and traveled distances (*G*) as compared with the TBI group. $^{*}P < 0.05$, $^{**}P < 0.01$ (One-way ANOVA with multiple comparisons test, $n = 11$–12 mice/group). Data represent the mean ± SEM.

we provide anatomical and functional evidence showing that ZL006 reduces neuronal loss, tissue damage and improves sensorimotor, memory, and cognitive recoveries after TBI. These findings collectively suggest that modulation of the nNOS–PSD95 interaction could represent a new therapeutic strategy for treating TBI.

Excessive stimulation of NMDARs and the resulting nNOS activation are crucial for neural injury and subsequent morbidity and mortality after TBI (Gahm et al. 2005; Sharma et al. 2006; Han et al. 2009). There is much evidence in the literature linking glutamate excitotoxicity to NO signaling, connecting nNOS and PSD95 binding to enhanced calcium influx leading to neuronal toxicity and death (Huang et al. 1994; Dawson et al. 1996; Sattler et al. 1999). To confirm the efficacy of ZL006 in minimizing excitotoxic neuronal injury and death, we investigated the effect of ZL006 pre- and post-treatment on glutamate toxicity in isolated cortical neuronal cultures. Our findings showed that this treatment disrupted nNOS–PSD95 interaction and protected cortical neurons from glutamate-induced excitotoxicity in a dose dependent manner (Fig. 1), suggesting disrupting the nNOS–PSD95 interaction can block NMDAR activation-induced neuronal death. In agreement with our observation, a recent report showed that disrupting nNOS–PSD95 with ZL006 or overexpression of N-terminal amino acid residues 1–133 of nNOS had neuroprotective effect against glutamate-induced cultured cortical neuronal death (Zhou et al. 2010).

Apoptosis has been considered as a key mechanism of cell death following TBI (Raghupathi et al. 2000; Raghupathi 2004; Stoica and Faden 2010). Caspase-3 plays a central role in the execution phase of apoptosis and is responsible for the cleavage of proteins such as the nuclear enzyme PARP. The ratio of Bcl-2/Bax determines survival or death of cells following an apoptotic stimulus (Oltvai et al. 1993). Our results showed that TBI induced expression of active caspase-3 and PARP-1, and increased ratio of Bcl-2/Bax (Fig. 2*B*–*D*). TUNEL staining further confirmed neuronal apoptosis after the TBI (Fig. 2*E*–*J*), supporting the notion that glutamate and NO induces neural apoptosis (Palluy and Rigaud 1996; Ghatan et al. 2000; Zhang and Bhavnani 2005, 2006). A striking finding of this study is that administration of ZL006 at 30 min postinjury (10 mg/kg, i.p.) significantly reduced TBI-induced nNOS–PSD95 complex and neuronal apoptosis (Fig. 2), consistent with a recent report that ZL006 protected oxygen and glucose deprivation-induced neuronal apoptosis (Liu et al. 2017). Importantly, our coimmunoprecipitation assay provide

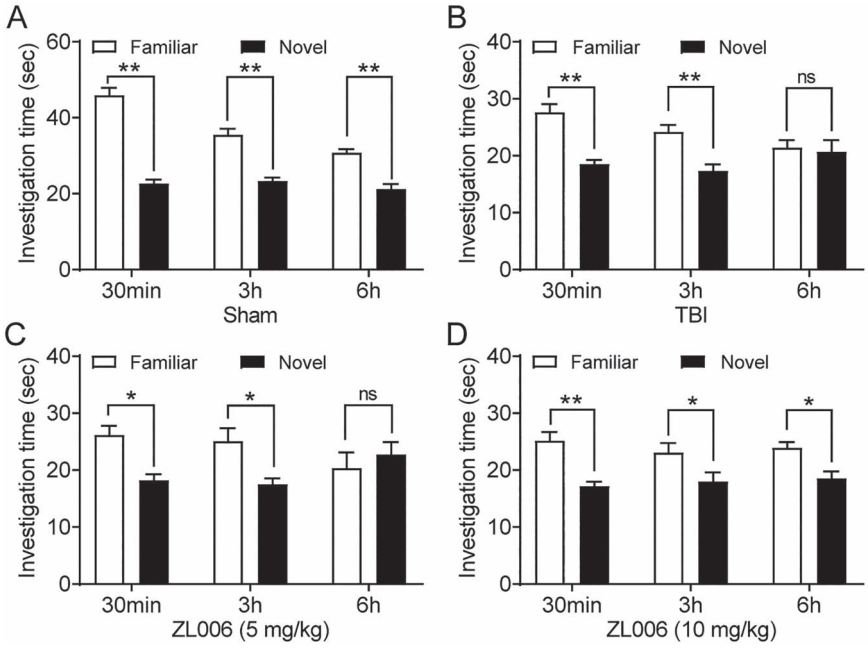

Figure 6. ZL006 improves social memory following TBI. (*A*) Mice in sham group spent significantly more time with the familiar than the novel stimulus mouse at three test time intervals. (*B*) TBI group showed abnormal (no difference) social interaction at the 6 h interval, suggesting deficits in social memory. (*C*) Mice receiving ZL006 treatment at 5 mg/kg (i.p.) also displayed deficits in social memory at the 6 h interval. (*D*) Mice receiving ZL006 treatment at 10 mg/kg (i.p.) displayed normal social interaction and memory as the sham group, that is, spent significantly more time with the familiar than the novel stimulus mouse at all three test time intervals. $^{*}P < 0.05$, $^{**}P < 0.01$, ns, not significant (two-way repeated measures ANOVA with multiple comparisons test, $n = 11$ mice/group). Data represent the mean ± SEM.

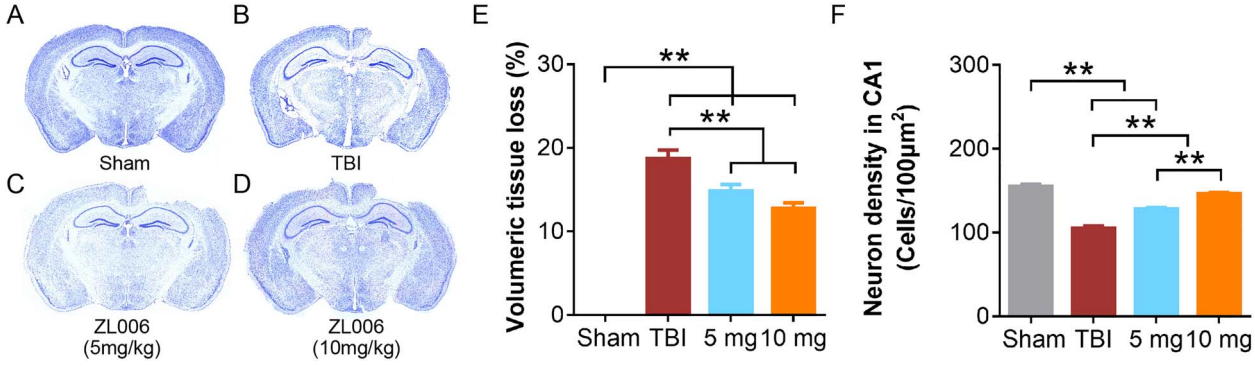

Figure 7. ZL006 reduces cortical tissue damage following TBI. (*A–D*) Cresyl violet-stained sections show ZL006 reduced cortical tissue loss at 4 weeks after TBI. (*E*) A bar graph shows that ZL006 treatment significantly reduced percent volumetric tissue loss in the injured cortex in a dose-dependent manner at 4 weeks after TBI. (*F*) ZL006 treatment significantly reduced neuronal loss in the CA1 region of hippocampus in a dose-dependent manner at 4 weeks after TBI. $^{**}P < 0.01$ (one-way ANOVA with multiple comparisons test, $n = 11$–12 mice/group). Data represent the mean ± SEM.

direct evidence of ZL006's disruption of nNOS–PSD95 complex which was increased after TBI, consistent with the observation reported that ZL006 inhibited the increase in nNOS–PSD95 complex in neurons activated by glutamate and in cortices of nNOS+/+, but not nNOS−/− mice with cerebral ischemia (Zhou et al. 2010).

The activation of p38 MAPK is a known participant in acute neuronal death pathways following CNS injuries, and its downregulation has been shown to be neuroprotective (Tikka et al. 2001; Yang et al. 2017). NMDAR activation leads to p38 MAP kinase activation and neuronal death (Wu and Tymianski 2018). NO-induced activation of p38 MAP kinase has been shown to promote Bax translocation to mitochondria and cause cell death, which is not blocked by caspase inhibitors (Ghatan et al. 2000). We examined p-p38 expression in penumbral cortex neurons through immunofluorescent colocalization and observed a reduction in p-p38-positive neurons following the ZL006 treatment (10 mg/kg) (Fig. 3A–J). In addition, Western blot analysis showed a reduction of p38 in the cortical tissue of TBI mice treated with ZL006 (Fig. 3K). Since nNOS–PSD95 interaction and subsequently NO production are critical for glutamate-induced p38 activation and neuronal death (Cao et al. 2005), blocking this series of events with ZL006 would likely prevent glutamate-induced cell death and promote neurological recoveries.

A significant finding of this study is that pharmacological disruption of nNOS–PSD95 interaction with ZL006 reduced neuronal loss, tissue damage, and promoted recovery of sensorimotor, memory, and cognitive functions in C57BL/6 mice after TBI (Fig. 4–7). Notably, the ZL006 was administered after trauma and the treatment showed a long beneficial effect on anatomical and

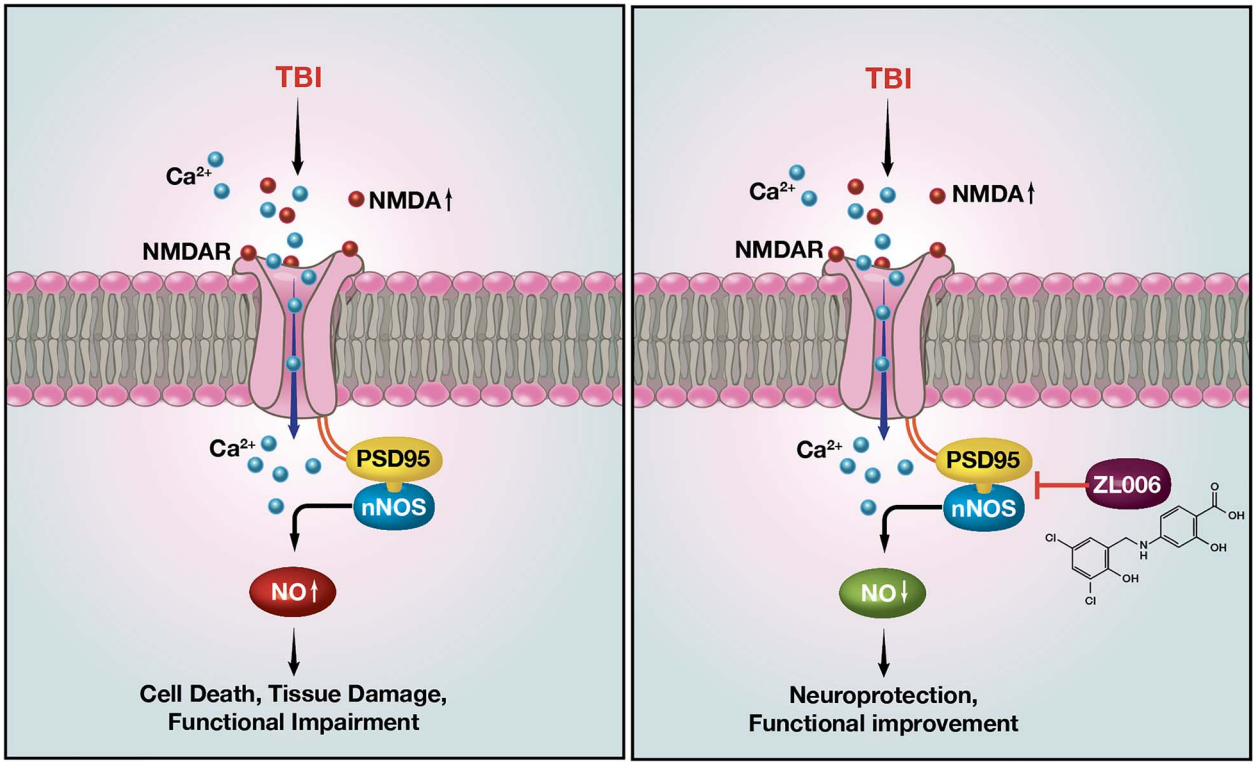

Figure 8. Diagram depicting NMDAR–NO signaling pathway and proposed mechanism of ZL006 inhibition on nNOS and PSD95 interaction after TBI. (*A*) Following TBI, NMDAR is activated and nNOS is coupled to the postsynaptic scaffolding protein PSD-95, thus positioning nNOS for a more effective activation and production of NO by calcium influx through the NMDAR channel pore, leading to increased neuronal death, tissue damage and functional impairments. (*B*) Disruption of nNOS–PSD95 interaction with ZL006 reduces the NMDA-induced production of NO, and hence decreases NO-mediated neuronal death, tissue damage, and functional deficits.

functional recoveries. Although no obvious tissue damage was detected in the hippocampus, neuronal loss in the CA1 region was found. Importantly, ZL006 administration significantly reduced neuronal loss in the CA1 region, suggesting that such reduction of neuronal loss may be associated with improvements in spatial memory and learning, measured by Morris Water Maze, in the ZL006 treatment group as compared with the nontreatment group. In agreement with our observation, ZL006 disrupted ischemia-induced nNOS–PSD95 interaction selectively, had potent neuroprotective activity in vitro, and ameliorated focal cerebral ischemic damage in mice and rats subjected to middle cerebral artery occlusion and reperfusion (Zhou et al. 2010). Disruption of nNOS–PSD95 complex by ZL006 also promoted neuronal differentiation of neural stem cells in the ischemic brain of rats and improved stroke outcome even when administered during recovery stage of ischemia (i.e., 4 days after stroke) (Luo et al. 2014). Our study provides new knowledge that nNOS–PSD95 complex contributes to the pathogenesis of TBI and that targeting the nNOS–PSD95 complex could be an effective therapeutic strategy for intervention after TBI.

With the overall benefits observed following ZL006 treatment in the present study, the foundation has been laid for future optimization of treatment, including identifying optimal time windows of the treatment, possible dosing modifications to improve benefits, and refining our understanding of the drug's mechanisms of action. In addition, future analyses will include assessment of the effects of ZL006 on other cell types, including astrocytes, microglia, and vasculature within the brain, all of which are known to be affected by trauma following injury.

Funding

NIH 1R01 NS100531, 1R01 NS103481, Merit Review Award I01 BX002356, I01 BX003705 from the U.S. Department of Veterans Affairs; Indiana Spinal Cord and Brain Injury Research Foundation (No. 19919); Mari Hulman George Endowment Funds (to X.M.X.); ISDH (Grant# A70-2-079609 and A70-9-079138 to N.K.L.); R21 MH104018 (to A.S.).

Notes

We thank Patti Raley, a medical editor, for critical reading of the manuscript; and Herqiao Dai, a technician, for his technical assistance. We thank Dr Wei Yang for her assistance on the manuscript. We are grateful for the use of the Core facility of the Spinal Cord and Brain Injury Research Group/Stark Neurosciences Research Institute at Indiana University. *Conflict of Interest*: None declared.

Author Contributions

W.Q., N.K.L., Y.L., A.S., X.M.X. contributed to the conception and design of the study; W.Q., N.K.L., X.W., Y.W., Y.X., Y.S. contributed to the acquisition and analysis of data; W.Q., N.K.L., R.L., A.S., X.M.X. contributed to drafting the text and preparing the figures.

References

Cai J, Zhong YW, Li F, Wang SZ. 2011. Anti-amyloid beta single-chain Fv ameliorates behavioral impairment in Alzheimer's

disease mice via adeno-associated virus delivery. *Neural Regen Res*. 6:96–100.

Cao J, Viholainen JI, Dart C, Warwick HK, Leyland ML, Courtney MJ. 2005. The PSD95-nNOS interface: a target for inhibition of excitotoxic p38 stress-activated protein kinase activation and cell death. *J Cell Biol*. 168:117–126.

Castillo J, Rama R, Davalos A. 2000. Nitric oxide-related brain damage in acute ischemic stroke. *Stroke*. 31:852–857.

Chizh BA, Headley PM. 2005. NMDA antagonists and neuropathic pain—multiple drug targets and multiple uses. *Curr Pharm Des*. 11:2977–2994.

Coggeshall RE. 1992. A consideration of neural counting methods. *Trends Neurosci*. 15:9–13.

Dawson VL, Kizushi VM, Huang PL, Snyder SH, Dawson TM. 1996. Resistance to neurotoxicity in cortical cultures from neuronal nitric oxide synthase-deficient mice. *J Neurosci*. 16:2479–2487.

Gahm C, Danilov A, Holmin S, Wiklund PN, Brundin L, Mathiesen T. 2005. Reduced neuronal injury after treatment with NG-nitro-L-arginine methyl ester (L-NAME) or 2-sulfophenyl-N-tert-butyl nitrone (S-PBN) following experimental brain contusion. *Neurosurgery*. 57:1272–1281, discussion 1272–1281.

Ghatan S, Larner S, Kinoshita Y, Hetman M, Patel L, Xia Z, Youle RJ, Morrison RS. 2000. p38 MAP kinase mediates bax translocation in nitric oxide-induced apoptosis in neurons. *J Cell Biol*. 150:335–347.

Han RZ, Hu JJ, Weng YC, Li DF, Huang Y. 2009. NMDA receptor antagonist MK-801 reduces neuronal damage and preserves learning and memory in a rat model of traumatic brain injury. *Neurosci Bull*. 25:367–375.

Han S, Zhang KH, Lu PH, Xu XM. 2004. Effects of annexins II and V on survival of neurons and astrocytes in vitro. *Acta Pharmacol Sin*. 25:602–610.

Huang Z, Huang PL, Panahian N, Dalkara T, Fishman MC, Moskowitz MA. 1994. Effects of cerebral ischemia in mice deficient in neuronal nitric oxide synthase. *Science*. 265:1883–1885.

Lai TW, Zhang S, Wang YT. 2014. Excitotoxicity and stroke: identifying novel targets for neuroprotection. *Prog Neurobiol*. 115:157–188.

Lee WH, Xu Z, Ashpole NM, Hudmon A, Kulkarni PM, Thakur GA, Lai YY, Hohmann AG. 2015. Small molecule inhibitors of PSD95-nNOS protein-protein interactions as novel analgesics. *Neuropharmacology*. 97:464–475.

Li LP, Dustrude ET, Haulcomb MM, Abreu AR, Fitz SD, Johnson PL, Thakur GA, Molosh AI, Lai Y, Shekhar A. 2018. PSD95 and nNOS interaction as a novel molecular target to modulate conditioned fear: relevance to PTSD. *Transl Psychiatry*. 8:155.

Liu N, Han S, Lu PH, Xu XM. 2004. Upregulation of annexins I, II, and V after traumatic spinal cord injury in adult rats. *J Neurosci Res*. 77:391–401.

Liu NK, Deng LX, Zhang YP, Lu QB, Wang XF, Hu JG, Oakes E, Bonventre JV, Shields CB, Xu XM. 2014a. Cytosolic phospholipase A2 protein as a novel therapeutic target for spinal cord injury. *Ann Neurol*. 75:644–658.

Liu NK, Zhang YP, O'Connor J, Gianaris A, Oakes E, Lu QB, Verhovshek T, Walker CL, Shields CB, Xu XM. 2013. A bilateral head injury that shows graded brain damage and behavioral deficits in adultmice. *Brain Res*. 1499:121–128.

Liu NK, Zhang YP, Zou J, Verhovshek T, Chen C, Lu QB, Walker CL, Shields CB, Xu XM. 2014b. A semicircular controlled cortical impact produces long-term motor and cognitive dysfunction that correlates well with damage to both the sensorimotor cortex and hippocampus. *Brain Res*. 1576:18–26.

Liu SG, Wang YM, Zhang YJ, He XJ, Ma T, Song W, Zhang YM. 2017. ZL006 protects spinal cord neurons against ischemia-induced oxidative stress through AMPK-PGC-1alpha-Sirt3 pathway. *Neurochem Int*. 108:230–237.

Loane DJ, Faden AI. 2010. Neuroprotection for traumatic brain injury: translational challenges and emerging therapeutic strategies. *Trends Pharmacol Sci*. 31:596–604.

Luo CX, Lin YH, Qian XD, Tang Y, Zhou HH, Jin X, Ni HY, Zhang FY, Qin C, Li F *et al*. 2014. Interaction of nNOS with PSD-95 negatively controls regenerative repair after stroke. *J Neurosci*. 34:13535–13548.

Maccallini C, Amoroso R. 2016. Targeting neuronal nitric oxide synthase as a valuable strategy for the therapy of neurological disorders. *Neural Regen Res*. 11:1731–1734.

Martos YV, Braz BY, Beccaria JP, Murer MG, Belforte JE. 2017. Compulsive social behavior emerges after selective ablation of striatal cholinergic interneurons. *J Neurosci*. 37:2849–2858.

McIntosh TK, Smith DH, Meaney DF, Kotapka MJ, Gennarelli TA, Graham DI. 1996. Neuropathological sequelae of traumatic brain injury: relationship to neurochemical and biomechanical mechanisms. *Lab Investig*. 74:315–342.

Morris RG, Garrud P, Rawlins JN, O'Keefe J. 1982. Place navigation impaired in rats with hippocampal lesions. *Nature*. 297:681–683.

Oltvai ZN, Milliman CL, Korsmeyer SJ. 1993. Bcl-2 heterodimerizes in vivo with a conserved homolog, Bax, that accelerates programmed cell death. *Cell*. 74:609–619.

Palluy O, Rigaud M. 1996. Nitric oxide induces cultured cortical neuron apoptosis. *Neurosci Lett*. 208:1–4.

Parsons CG. 2001. NMDA receptors as targets for drug action in neuropathic pain. *Eur J Pharmacol*. 429:71–78.

Raghupathi R. 2004. Cell death mechanisms following traumatic brain injury. *Brain Pathol*. 14:215–222.

Raghupathi R, Graham DI, McIntosh TK. 2000. Apoptosis after traumatic brain injury. *J Neurotrauma*. 17:927–938.

Regasa LE, Agimi Y, Stout KC. 2018. Traumatic brain injury following military deployment: evaluation of diagnosis and cause of injury. *J Head Trauma Rehabil*.

Sattler R, Xiong Z, Lu WY, Hafner M, MacDonald JF, Tymianski M. 1999. Specific coupling of NMDA receptor activation to nitric oxide neurotoxicity by PSD-95 protein. *Science*. 284: 1845–1848.

Sharma HS, Wiklund L, Badgaiyan RD, Mohanty S, Alm P. 2006. Intracerebral administration of neuronal nitric oxide synthase antiserum attenuates traumatic brain injury-induced blood-brain barrier permeability, brain edema formation, and sensory motor disturbances in the rat. *Acta Neurochir Suppl*. 96:288–294.

Stoica BA, Faden AI. 2010. Cell death mechanisms and modulation in traumatic brain injury. *Neurotherapeutics*. 7:3–12.

Taylor CA, Bell JM, Breiding MJ, Xu L. 2017. Traumatic brain injury-related emergency department visits, hospitalizations, and deaths—United States, 2007 and 2013. *MMWR Surveill Summ*. 66:1–16.

Thor DH, Holloway WR Jr. 1986. Caffeine and copulatory experience: interactive effects on social investigatory behavior. *Physiol Behav*. 36:707–711.

Tikka T, Fiebich BL, Goldsteins G, Keinanen R, Koistinaho J. 2001. Minocycline, a tetracycline derivative, is neuroprotective against excitotoxicity by inhibiting activation and proliferation of microglia. *J Neurosci*. 21:2580–2588.

Wu QJ, Tymianski M. 2018. Targeting NMDA receptors in stroke: new hope in neuroprotection. *Mol Brain*. 11:15.

Yang H, Gu ZT, Li L, Maegele M, Zhou BY, Li F, Zhao M, Zhao KS. 2017. SIRT1 plays a neuroprotective role in traumatic brain injury in rats via inhibiting the p38 MAPK pathway. *Acta Pharmacol Sin*. 38:168–181.

Yang L, Zou B, Xiong X, Pascual C, Xie J, Malik A, Xie J, Sakurai T, Xie XS. 2013. Hypocretin/orexin neurons contribute to hippocampus-dependent social memory and synaptic plasticity in mice. *J Neurosci*. 33:5275–5284.

Zhang Y, Bhavnani BR. 2005. Glutamate-induced apoptosis in primary cortical neurons is inhibited by equine estrogens via down-regulation of caspase-3 and prevention of mitochondrial cytochrome c release. *BMC Neurosci*. 6:13.

Zhang Y, Bhavnani BR. 2006. Glutamate-induced apoptosis in neuronal cells is mediated via caspase-dependent and independent mechanisms involving calpain and caspase-3 proteases as well as apoptosis inducing factor (AIF) and this process is inhibited by equine estrogens. *BMC Neurosci*. 7: 49.

Zhou L, Li F, Xu HB, Luo CX, Wu HY, Zhu MM, Lu W, Ji X, Zhou QG, Zhu DY. 2010. Treatment of cerebral ischemia by disrupting ischemia-induced interaction of nNOS with PSD-95. *Nat Med*. 16:1439–1443.